THE JOURNAL OF PHYSICAL CHEMISTRY C

Article

pubs.acs.org/JPCC

In Situ Spectroelectrochemical Determination of Energy Levels and Energy Level Offsets in Quantum-Dot Heterojunctions

Simon C. Boehme,*[,†,∥] Daniël Vanmaekelbergh,[‡] Wiel H. Evers,[†,§] Laurens D. A. Siebbeles,[†] and Arjan J. Houtepen*[,†]

[†]Chemical Engineering, Optoelectronic Materials, Delft University of Technology, Julianalaan 136, 2628 BL Delft, The Netherlands

[‡]Debye Institute, Condensed Matter and Interfaces, Utrecht University, P.O. Box 80.000, 3508 TA Utrecht, The Netherlands

[§]Kavli Institute of Nanoscience, Delft University of Technology, P.O. Box 5046, 2600 GA Delft, Netherlands

Supporting Information

ABSTRACT: Charge transfer in semiconductor heterojunctions is largely governed by the offset in the energy levels of the constituent materials. Unfortunately, literature values for such energy level offsets vary widely and are usually based on energy levels of the individual materials rather than of actual heterojunctions. Here we present a new method to determine absolute energy levels and energy level offsets in situ for films containing CdSe and PbSe quantum dots. Using spectroelectrochemistry, we find a type I offset at the CdSe-PbSe heterojunction. Whereas the energy level offset follows the expected size-dependent trend, the absolute positions of the $1S_e$ level in the individual CdSe or PbSe quantum dots does not. This level varies by more than 0.5 eV, depending on film composition and surface defect concentration. Rather than extrapolating energy level offsets from measurements on pure CdSe or PbSe quantum-dot films, we suggest measuring energy level offsets in heterojunctions in situ.

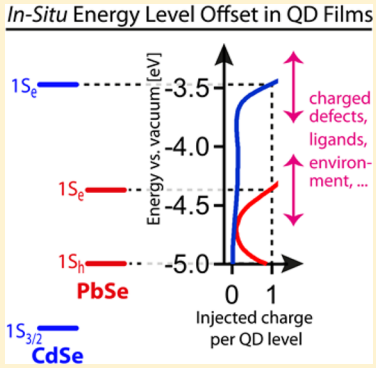

1. INTRODUCTION

Charge transfer at an interface is a fundamental process in many electronic devices, as it allows one to separate charge carriers and guide them into different spatial domains. To this end, many device designs employ a semiconductor heterojunction comprised of two distinct materials, such as a donor−acceptor (D-A) junction. Upon photoexcitation, disparate energy levels in the conduction and valence band of donor and acceptor lead to transfer of electrons and holes. In case of a staggered or type II band alignment (i.e., with one side of the interface possessing both the larger electron affinity and ionization potential), this allows charge separation: electrons and holes accumulate at opposite sides of the interface. To control the direction of charge transfer, knowledge of absolute and relative energy levels in the heterojunction is of paramount importance.

A large experimental toolbox is available to determine charge transfer rates, including ultrafast pump−probe spectroscopy.[1−7] The observed rates are then described employing a theoretical model that often involves the energy difference between donor and acceptor, such as in the Marcus theory.[8−11] It would therefore be insightful to experimentally determine this energy difference. This would enable the experimental verification of the employed charge transfer models and the prediction of charge transfer rates in new material combinations. Hence, a method to measure energy level offsets would be very helpful for the directed design of devices.

Unfortunately, realization of this concept is hindered by the fact that literature values for absolute energy levels vary by more than 1 eV, often exceeding typical energy differences between materials in heterojunctions. This can be explained in part by the different experimental techniques that were used. Each of them has its own pitfalls: for example, optical spectroscopy (such as intraband spectroscopy on core/shell heterostructures)[12] inherently probes both electron and hole states. Ultraviolet photoelectron spectroscopy (UPS),[13] photoelectron spectroscopy in air (PESA),[14] and Kelvin probe measurements[15] only access the surface of a sample. The assessment of the energetics at distances more than a few nanometers away from the surface is generally not possible. In addition, measurements are often performed under vacuum, probing energy levels in a different environment than present in the final device.

Electrochemical measurements such as the commonly employed cyclic voltammetry (CV) technique offer an alternative approach:[16−19] films exceeding one micrometer in thickness can easily be measured if the film is sufficiently porous to allow penetration of electrolyte ions.[17,20] In CV measurements, the potential applied to the sample is scanned in a cyclic fashion and energy levels are assigned on the basis of anodic and cathodic peaks in the charging current. However, this film capacitance represents the total density of states and includes localized (surface)-defect states, complicating the study of the electronic structure. Localized surface states can

Received: December 8, 2015
Revised: February 11, 2016
Published: February 16, 2016

DOI: 10.1021/acs.jpcc.5b12016
J. Phys. Chem. C 2016, 120, 5164−5173

often be distinguished from delocalized conduction or valence band states by their optical activity.[21] The latter are involved in strong optical transitions, while surface and defect states are not. A simultaneous detection of the optical and/or electrical properties induced by charge carrier injection is thus helpful. Such spectroelectrochemical techniques that combine electrochemical charging with photoluminescence or absorption spectroscopy have been very successful in understanding the density of states of quantum dot (QD) films.[16−18] Still, the presence of charged QD surfaces or heterojunction interfaces strongly influences the energy levels. It is therefore preferred to measure energy level offsets in situ on the actual heterojunction samples of interest.

Here, we present results of spectroelectrochemical measurements on films of CdSe and PbSe QDs. Charges injected into quantum-confined energy levels bleach the absorption due to interband transitions to/from this level.[22] The voltage at which such absorption changes occur can then be directly converted to an absolute energy scale by calibration of the potential of the reference electrode. This approach readily allows to determine the ($1S_e$) quasi-particle energy level, i.e., the potential at which one electron occupies the ($1S_e$) level. This is the most relevant quantity for the study of charge transfer and charge transport as well as the utilization of these processes in devices: it is the energy that needs to be paid for injecting or transferring an electron to the $1S_e$ level. Furthermore, spectroelectrochemistry enables the in situ determination of the CdSe-PbSe QD energy level offset in a heterojunction comprised of both materials: since the CdSe and PbSe QDs feature different band gaps, one can distinguish electrons occupying the eigenstates of CdSe from those in PbSe QDs.

We electrochemically inject charges in films of PbSe and CdSe QDs and simultaneously monitor the bleaching of interband transitions to determine the absolute energy of their respective $1S_e$ levels. Next, we fabricate composite films containing both type of QDs to determine their energy level offset in situ and discuss the dependence on the dielectric environment. We show that the $1S_e$ conduction level of PbSe QDs is always below that of CdSe QDs, consequently forming a type I heterojunction. We find that the absolute energy levels of the QDs are very sensitive to surface charging, but that the energy level offset between them is mostly unaffected. The energy level offset found by *in situ* measurements is however significantly larger than the offset expected from measurements on reference films of PbSe QDs or CdSe QDs only. This highlights the importance of *in situ* measurements for the determination of energy level offsets. The variations in the absolute energy levels are discussed in term of surface charging.

2. EXPERIMENTAL SECTION

2.1. QD Synthesis. CdSe QDs were synthesized following the procedure by Mekis et al.:[23] QDs with a diameter of 9.7 nm were obtained, as determined from the 1S peak of their absorption spectra and the sizing curve given by de Mello Donegá and Koole.[24] PbSe QDs of three different size (S, M, and L, with diameters of 4.1, 5.3, and 6.0 nm, respectively) were synthesized following the recipe by Steckel at al.[25] A first synthesis yielded QDs of size S and M. A second synthesis yielded QDs of size L.

2.2. Film Processing and Ligand Exchange. All QD films were grown on ITO substrates in a layer-by-layer (LbL) dip coating procedure in a N_2 purged glovebox: the substrates were first immersed for 30 s in a QD dispersion with a QD concentration on the order of 10^{-5} M, subsequently immersed for 30 s in a stirred 0.1 M solution of 1,6-hexanedithiol (6DT) ligands in MeOH, and finally dipped twice for 10 s in stirred MeOH to rinse excess ligands. Using this procedure, the original insulating ligands are replaced by the shorter bidentate ligands to allow for charge transport between QDs. Even shorter ligands than 6DT were not suited for electrochemical measurements as they result in films with voids too small for electrolyte ion penetration.[20] The above procedure was repeated 10−20 times to yield films roughly 10−20 QD monolayers thick. A small region on the edge of the ITO substrate remained uncoated to provide electrical contact in electrochemical measurements.

2.3. Electrochemical Control of the Fermi Level. Spectroelectrochemical measurements were performed according to the procedure described previously.[20] In short, QD films were immersed in an airtight Teflon container containing a 0.1 M $LiClO_4$ electrolyte in acetonitrile, a Ag wire pseudoreference electrode and a Pt sheet counter electrode. The potential of the QD film on ITO was controlled with CHI832B bipotentiostat (CH Instruments, Inc.). Potential dependent changes in the absorption of the QD film were recorded simultaneously with a UV−vis spectrometer (USB2000, Ocean Optics) and a near-IR spectrometer (NIRQuest 256, Ocean Optics), with a combined range of about 400 to 2400 nm (3.1 to 0.5 eV). This way, the band edge transition of both PbSe and CdSe QDs can be acquired simultaneously. For all films, the potential was scanned in a cyclic fashion (CV mode), starting from open circuit potential (inside band gap, usually close to 0 V), scanning at a rate of 10 mV/s, first in negative direction (toward the $1S_e$ level), and repeating a cycle two to three times. Absorption difference spectra (with respect to the absorption at open circuit potential) were taken every 10−20 mV and the acquired spectra during the first leg of the first cycle are shown in the figures of the results section. A correction for a spectrally broad induced absorption is applied as shown in the Supporting Information. Unless stated otherwise, all potentials are given with respect to a Ag wire pseudoreference electrode immersed in the electrolyte. Its potential (−4.75 eV vs vacuum) was calibrated with a ferrocene/ferrocinium couple[26,27] and was stable within 20 meV. The convention was used that a negative potential corresponds to a shift of the sample's Fermi level toward vacuum.

2.4. Differential Capacitance Measurements. To correct for Faradaic background currents in the electrolyte and to determine the steady-state capacitance, we perform differential capacitance measurements. To this end, we scan the potential in a step-like fashion. After each potential step (of 50 mV), we record the electrochemical charging current, i.e., the current between sample and a Pt sheet counter electrode. The initial peak current quickly decays to an almost constant level within the first 0.5 s following the step. Since the constant current after decay of the initial dynamics can be attributed to Faradaic background currents in the electrolyte, we subtract this constant level and obtain the current contribution due to electrochemical charging of the film. This background corrected current is integrated and divided by the potential step to yield the differential capacitance, in units of C/V. The differential capacitance is due to the conduction and valence band states in the QD, and due to the double layer capacitance of the QD film as well as the parts of the ITO substrate which are in direct contact with the electrolyte. To correct for the double layer

DOI: 10.1021/acs.jpcc.5b12016
J. Phys. Chem. C 2016, 120, 5164−5173

capacitance, we subtract a (potential independent) value of about 3×10^{-5} C/V for each film.

3. RESULTS AND DISCUSSION

3.1. Fermi Level Control. Figure 1 depicts a schematic of electrochemical charge injection into a QD film on a conductive substrate. The film is immersed in an electrolyte. The top panel illustrates the equilibrium situation, i.e., no voltage is applied between ITO and the (pseudo-) reference electrode. In this case, the Fermi level (E_F, dashed line) lies within the band gap and the QDs are uncharged. The bottom panel shows the situation when a voltage is applied between ITO and the reference electrode. If the voltage is sufficiently negative, the Fermi level is moved into the conduction band of the QD film and electrons are injected into the QDs. These charges are compensated by Li^+ cations penetrating the voids of the QD film. In the depicted case, every QD contains one electron on average, corresponding to a charge density on the order of 10^{18} to 10^{21} cm^{-3} for QDs with diameters ranging from 10 to 1 nm. This is considered the degenerate doping regime for conventional semiconductor devices.[28] Doping levels of up to ten charges per QD have been demonstrated by electrochemical charging, yielding information on both hole and electron quantum confined levels.[17,22,29,30] As Li^+ ions are uniformly distributed over the film, the energy levels are also constant over the entire film, i.e. no band bending occurs.

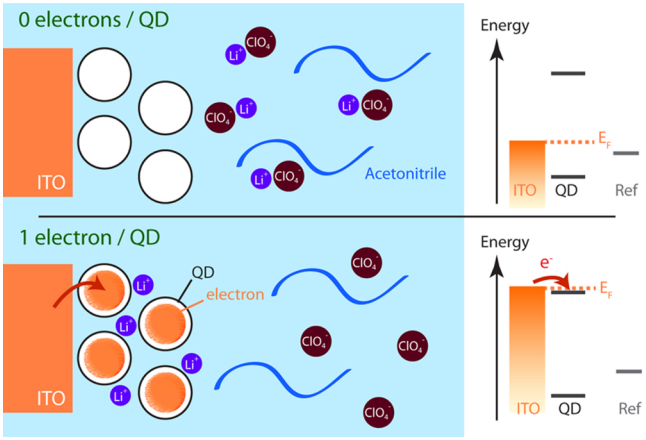

Figure 1. Schematic of electrochemical charge injection into a QD film on a conductive substrate (ITO), immersed in an electrochemical cell containing a solution of $LiClO_4$ in acetonitrile as the electrolyte. Top: at open circuit, the Fermi level (E_F) in the QDs is within the band gap and QDs are uncharged. Bottom: if the Fermi level in the ITO is raised sufficiently by applying a voltage between the ITO and the reference electrode (ref), electrons are injected into the QDs. As a response, Li^+ cations will penetrate the voids in the QD film to compensate the injected charge. Since the QDs are small compared to typical depletion widths, no band bending occurs and the energy levels are constant throughout the film. Here, the situation of one electron per QD is depicted.

This presents a major difference to Field Effect Transistors (FETs), where only planar charge compensation is provided and depletion regions form. As a consequence, the gate coupling (i.e., the ratio between effective shift of the Fermi level and applied voltage) is low in FETs. In contrast, as has been shown earlier[16−18] and as we show later, the gate coupling is close to unity in the electrolyte-gated devices. This means that the electrochemical potential of charge injection in the electrolyte-gated device directly reflects the quasi-particle energy levels of QD films (see the Supporting Information).

3.2. Ground-State Absorption. PbSe and CdSe QDs were synthesized as outlined in the Experimental Section. We use CdSe QDs of a single size (9.7 nm in diameter) and PbSe QDs of three sizes: 4.1, 5.3, and 6.0 nm diameter, labeled S, M, and L, respectively. Thin films were made from these QDs via a layer-by-layer approach using a mechanical dipcoater (see Experimental Section). This allows the formation of smooth thin films of either the pure QD materials, or composite films. The composite films are either bilayer films (approximately 10 layers of CdSe QDs on top of 10 layers of PbSe QDs) or multilayer structures where monolayer of CdSe and PbSe QDs are alternating.

Figure 2 displays the absorption spectra of all QD films studied in this article. In the top panel of Figure 2a, the absorbance of a film of PbSe QDs (of size M) is shown (blue solid line), below that the absorbance of a pure film of CdSe QDs (yellow solid line), and below that the absorbance of a bilayer comprising a film of CdSe QDs grown on top of a film of PbSe QDs of size M (green solid line). To separate the absorbance contribution of both types of QDs, a line is fitted to the bilayer spectrum from ~1.55 eV to ~1.75 eV and extrapolated to 2.5 eV to emulate the (almost featureless) PbSe contribution in the region from 1.9 to 2.5 eV (blue dotted line). Subtraction of this simulated PbSe contribution yields the CdSe contribution to the bilayer spectrum (light green solid line). In Figure 2b, the PbSe and CdSe contribution of composite films comprised of both types of QDs are shown, both around their respective 1S peak. Bilayers featuring CdSe QDs and PbSe QDs of size S, M, and L are shown as blue,

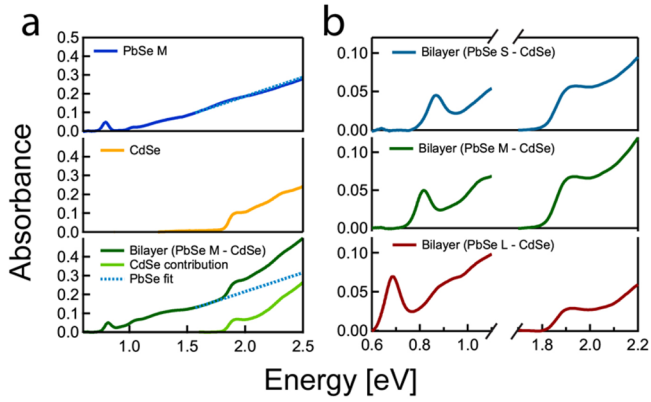

Figure 2. Absorption spectra of pure and composite QD films with 6DT ligands, comprising PbSe QDs of three different sizes and CdSe QDs of 9.7 nm. (a) Top: Film of PbSe QDs only (5.3 nm, size M, with 1S peak at 0.78 eV), depicted as dark blue solid line. A linear fit to the almost featureless absorption above 1.5 eV is shown as a light blue dotted line. Middle: Film of CdSe QDs only (9.7 nm, with 1S peak at 1.91 eV). Bottom: Bilayer (dark green solid line) consisting of a film of CdSe QDs on top of a film of PbSe QDs of size M. A (light blue dotted) line was fit to the spectrum to emulate the (almost featureless) PbSe contribution above 1.5 eV. Subtraction of the extrapolated PbSe contribution yields the CdSe contribution to the spectrum (light green solid line). (b) PbSe and CdSe QD contributions to the absorption of the bilayer QD films studied in this article. Top: Bilayer with PbSe QDs of size S (4.1 nm, with 1S peak at 0.91 eV). Middle: Bilayer with PbSe QDs of size M (5.3 nm, with 1S peak at 0.78 eV). Bottom: Bilayer with PbSe QDs of size L (6.0 nm, with 1S peak at 0.71 eV).

DOI: 10.1021/acs.jpcc.5b12016
J. Phys. Chem. C 2016, 120, 5164−5173

green, and red solid lines, respectively. All composite films show very similar CdSe 1S maxima, at 1.91 ± 0.05 eV.

3.3. Spectroelectrochemical Assessment of the $1S_e$ Electron Level in Films of PbSe QDs. We begin by assessing the quasi-particle energy levels in a film with PbSe QDs of 5.3 nm diameter (size M). Its absorption spectrum is shown in the top panel of Figure 3a. A pronounced peak at 0.795 eV due to the $1S_h1S_e$ transition as well as a small feature at 1.02 eV is observed which has been assigned to the $1P_h1P_e$ transition.[31] After the sample has been placed inside an electrochemical cell, the Fermi level in the sample is raised by applying a negative voltage between sample and Ag pseudoreference electrode. Starting from about −0.8 V, a bleach of the absorption ($\Delta A < 0$) at the $1S_h1S_e$ transition appears, see bottom panel in Figure 3a. The $1S_h1S_e$ bleach increases with voltage up to −1.1 V, reducing the absorption at the 1S peak by roughly 40% (i.e., close to 3 electrons in 8 levels), and then slightly decreases again for more negative voltages.

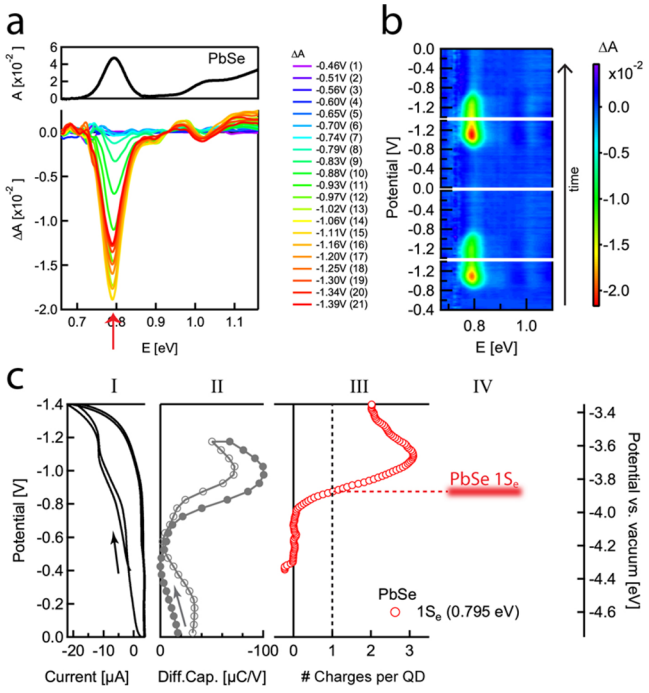

Figure 3. Spectroelectrochemical determination of the absolute energetic position of the $1S_e$ level in a film of 5.3 nm PbSe QDs (size M, 1S peak at 0.795 eV). (a) Upper half: ground state absorption spectrum. Lower half: differential absorption spectra for potentials ranging from midgap (−0.42 V) to −1.39 V, as given in the legend. No correction for a photoinduced absorption background was performed. The numbers in brackets indicate the acquisition order. (b) Differential absorption image obtained during the CV scan between 0 and −1.4 V, as given in panel I of (c). ΔA is displayed by false colors. Time runs from bottom to top. (c) Panel I: CV scan, starting from midgap (−0.42 V). An arrow indicates the scan direction. Panel II: differential capacitance on the forward scan (gray filled circles) and the backward scan (gray open circles). An arrow indicates the scan direction. Panel III: number of charges in the PbSe $1S_e$ level (red circles), as deduced from the relative absorption bleach $\Delta A/A$ at 0.795 eV. Panel IV: the energetic position of the $1S_e$ level at occupation by one electron is indicated by a horizontal bar. All potentials are given with respect to the Ag pseudoreference electrode (left axis) and vacuum (right axis).

Next to a bleach at the band edge, one observes a slight bleach at 0.9 eV and a red shift at 1.0 eV. The latter coincides with a peak in the linear absorption spectrum at the same energy, which we assign to the $1P_h1P_e$ transition. The former might be due to the formally (dipole-) forbidden $1S_h1P_e$ and $1P_h1S_e$ transitions.[31,32] Both the slight bleach at 0.9 eV and the red shift at 1.0 eV appear at the same voltage (about −0.8 V) as the band edge bleach, indicating that the filling of the $1S_e$ level is their cause.

After −1.4 V, the scan direction is reversed and the potential cycled twice between 0 and −1.4 V at a constant rate of 10 mV/s. Figure 3b shows the recorded differential absorbance as a false color image. The second CV cycle almost completely reproduces the absorption features of the first cycle, demonstrating that electrons can be reversibly and reproducibly injected into and extracted from the $1S_e$ level. However, a pronounced hysteresis is observed: on the backward scan, the bleach magnitude is lower and the potential of the bleach onset ill-defined. Moreover, the $1S_h1S_e$ bleach decreases again already before the potential scan direction is reversed, from about −1.1 V on the forward scan. Tentatively, we attribute the early bleach decrease and the hysteresis to slow trap filling at negative potentials. Such trap filling could lead to a reduction of the number of $1S_e$ electrons due to Coulomb repulsion among an increasing number of electrons in traps. As will be discussed below, we argue that filling of surface electron traps is the cause of significant variations in the energy levels of the QDs.

Figure 3c-I shows the simultaneously monitored electrochemical current in the CV scan, with an arrow indicating the scan direction and the potential at the start of the scan. Only one weakly pronounced reduction feature between −1.05 and −1.10 V is observed on the forward scan, while no oxidation feature could be resolved, in stark contrast to the strong optical absorption bleaches revealing filling and emptying of the $1S_e$ level. The cause of the absence of clear features in the CV is the presence of significant (Faradaic) background currents. These are always negative, irrespective of the scan direction and are attributed to reduction of solvent impurities and surface states. This highlights the added value of simultaneous collection of optical data for the determination of absolute energy levels.

As a control experiment, we further perform a differential capacitance measurement, i.e. we determine the amount of charge injected into the system after a small potential step of 50 mV (see experimental section for details). This quantity, in units of C/V and corrected for Faradaic background currents in the electrolyte, is depicted in Figure 3c-II. Filled and open gray circles show the differential capacitance for the forward and backward scan, respectively. A gray arrow indicates the scan direction and potential at start. At negative potentials exceeding −0.7 V, charge is injected into the QD film. At about −1.0 V, a peak of the differential capacitance is observed. The backward scan reproduces the forward scan, apart from a small difference in magnitude.

In order to investigate whether the differential capacitance reflects injection of electrons into the $1S_e$ level or injection into defect states in the band gap, we determine the number of $1S_e$ electrons $n_{1Se}(V)$ from the differential absorbance data in Figure 3a, depicted as red circles in Figure 3c-III. This number is inferred from the relative absorption bleach according to $n_{1Se}(V) = g_{1Se}\Delta A_{1Sh1Se}(V)/A_{1Sh1Se}(V_{oc})$, where g_{1Se} is the degeneracy of the $1S_e$ level (g_{1Se} = 8 in the case of PbSe[32]) and $\Delta A_{1Sh1Se}(V)$ is the differential absorbance at potential V with respect to the absorbance $A_{1Sh1Se}(V_{oc})$ at open circuit

DOI: 10.1021/acs.jpcc.5b12016
J. Phys. Chem. C 2016, 120, 5164−5173

potential V_{oc}. The number of $1S_e$ electrons are inferred from the (differential) absorbance at a photon energy of 0.795 eV, indicated by a red arrow in Figure 3a. From about −0.8 V, electrons are injected into the $1S_e$ level. At −0.87 V (corresponding to 3.88 eV below vacuum), an average population of one electron per QD is reached, indicated by a dashed vertical line. The population reaches a maximum of 3.1 electrons/QD at −1.09 V.

The derivative of the number of electrons per QD, $dn_{1Se}(V)/dV$, is the density of $1S_e$ states and should match the contribution of $1S_e$ injection to the differential capacitance shown in Figure 3c-II. Since the steepest slope in $n_{1Se}(V)$ is observed at a similar potential as the maximum in the differential capacitance, the differential capacitance predominantly reflects injection of $1S_e$ electrons. A second contribution to the differential capacitance might be due to (fast) reactions with solvent impurities or due to the filling of trap states. Traps in the band gap would explain the early onset of charge injection (at about −0.5 V), preceding the onset of the absorption bleach at about −0.75 V. Traps above the $1S_e$ level would explain that the maximum of the differential capacitance at −1.0 V is reached only after a maximum of $dn_{1Se}(V)/dV$ is observed at −0.9 V.

3.4. Spectroelectrochemical Assessment of Confined Electron Levels in Films of CdSe QDs. We proceed with the determination of electron energy levels in a film of CdSe QDs with a diameter of 9.7 nm. Figure 4a shows the absorption and differential absorption spectra of this film. Selected transitions are indicated by numbers 1−4, and assigned according to Norris and Bawendi:[33] feature 1 is due to the (closely spaced) $1S_{3/2}1S_e$ and $2S_{3/2}1S_e$ transitions, feature 2 is due to the $1P_{3/2}1P_e$ transition, feature 3 is due to the $3S_{1/2}1S_e$ transition and feature 4 is due to the $1P_{1/2}1P_e$, $1S_{1/2}2S_e$, and/or $4S_{3/2}2S_e$ transitions. At negative potentials exceeding −0.9 V, the absorption at transitions 1 and 3 starts to bleach simultaneously, as a result of the injection of electrons into the $1S_e$ level. At about −1.2 V, the first absorption peak is completely bleached and transitions 2 and 4 start to bleach, indicating the injection of electrons into the $1P_e$ level.

Figure 4b displays differential absorbance data of the entire CV scan as a false color image. Transitions 1 and 3, and 2 and 4 bleach and recover from bleaching in a concerted action. The differential absorbance for this sample clearly shows less hysteresis than for the PbSe QD film shown in Figure 3. This is likely due to less severe surface charging. Figure 4c depicts the electrochemical charging current during the CV scan (panel I), a differential capacitance scan (panel II), and the number of electrons in the $1S_e$ and $1P_e$ level as inferred from the differential absorbance (panel III). As in the case of the PbSe QD film, the CV scan lacks well-resolved reduction and oxidation features, while the differential capacitance reveals three pronounced injection regimes, marked by asterisks. The first regime (*) is not accompanied by optical changes (see panel III), suggesting the charging of trap states within the band gap or fast reactions with solvent impurities. The second regime (**) coincides with injection of $1S_e$ electrons as inferred from the bleaching of the $1S_{3/2}1S_e$ and $2S_{3/2}1S_e$ transition at 1.91 eV (dark blue line), and the third regime (***) coincides with injection of $1P_e$ electrons as inferred from the bleaching of the $1P_{3/2}1P_e$ transition at 2.06 eV (light blue line). This allows us to establish the quasi-particle energy diagram depicted in Panel IV: the energy corresponding to occupation of one electron per QD in the $1S_e$ level, i.e., $\Delta A_{1S3/2\rightarrow 1Se}(V)/A_{1S3/2\rightarrow 1Se}(0V) = -1/2$, resides at -3.68 eV vs vacuum. For the $1P_e$ level, the energy corresponding to occupation by one electron, i.e. $\Delta A_{1P3/2\rightarrow 1Pe}(V)/A_{1P3/2\rightarrow 1Pe}(0V) = -1/6$, lies 0.15 eV higher. The expected energy level difference can be estimated from the energy difference between the $1S_{3/2}1S_e$ and $1P_{3/2}1P_e$ transitions (0.15 eV) and the division of the optical energy over electron and hole levels using their respective effective masses of 0.13 and 0.44.[20] This results in an expected $1S_e$-$1P_e$ energy difference of 0.11 eV, in coarse agreement with the value of 0.15 eV found here.

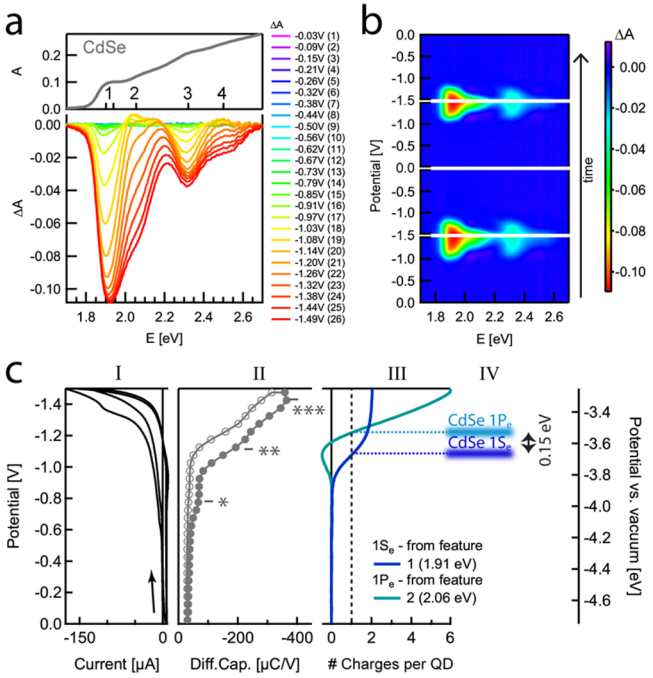

Figure 4. Spectroelectrochemical determination of the absolute energy of the $1S_e$ and $1P_e$ level in a film of 9.7 nm CdSe QDs (1S peak at 1.91 eV). (a) Upper half: ground state absorption spectrum. Lower half: differential absorption spectra for potentials ranging from open circuit potential (−0.03 V) to −1.49 V, as given in the legend. The numbers in brackets indicate the acquisition order. (b) Differential absorption image obtained during the CV scan between 0 and −1.5 V, as given in panel I of (c). ΔA is displayed by false colors. Time runs from bottom to top. (c) Panel I: CV, starting from open circuit potential (−0.03 V). An arrow indicates the scan direction. Panel II: differential capacitance. Filled gray circles depict the forward scan, empty gray circles the backward scan. A gray arrow indicates the scan direction. The three features (*), (**), and (***) are discussed in the main text. Panel III: optically derived number of charges in the CdSe $1S_e$ and $1P_e$ level. For the $1S_e$ level, this number is derived from the relative absorption bleach at transitions 1 (dark blue solid line), for the $1P_e$ level, it is deduced from the relative bleach at transition 3 (light blue solid line). Panel IV: absolute energies of the $1S_e$ and $1P_e$ levels.

3.5. Energy Level Offset in a PbSe QD/CdSe QD Heterostructure. Usually energy level offsets for heterojunctions are estimated based on the energy levels of the separate materials. If we do this for the PbSe and CdSe QD films discussed above, a $1S_e$ energy level offset of 0.2 eV would be expected. To investigate whether this offset is also found in in situ measurements on hetrojunction films we fabricated an alternating multilayer of both types of QDs by depositing a layer of PbSe QDs followed by a layer of CdSe QDs, and repeating this cycle 12 times. The absorption spectrum of the resulting film is shown as a black solid line in the top panel of Figure 5a. The estimated CdSe contribution (see the

DOI: 10.1021/acs.jpcc.5b12016
J. Phys. Chem. C 2016, 120, 5164−5173

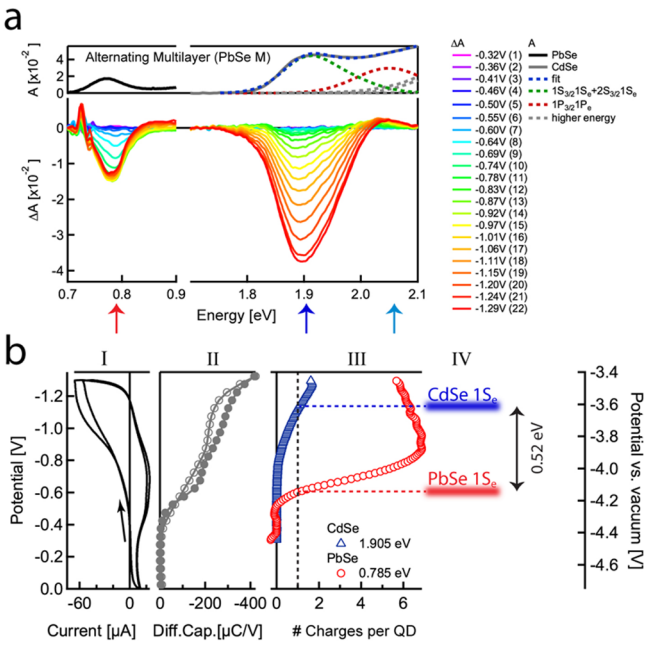

Figure 5. Spectroelectrochemical determination of the energy level offset in an alternating multilayer of 5.3 nm PbSe QDs (size M, 1S peak at 0.785 eV) and 9.7 nm CdSe QDs (1S peak at 1.905 eV). (a) Absorption (top) and differential absorption spectra at various potentials (bottom). The contribution of CdSe (gray solid line) to the absorption spectrum is obtained as described in the Experimental Section and fitted with a sum of 6 Gaussians (blue dashed line). Transitions involving the $1S_e$ and $1P_e$ levels are depicted by green and red dashed lines, respectively, and higher energy transitions by gray dashed lines. (b) Panel I: CV starting from −0.3 V. An arrow indicates the scan direction. Panel II: differential capacitance, starting from 0 V. Filled gray circles depict the forward scan, empty gray circles the backward scan. Panel III: optically derived number of charges in the PbSe $1S_e$ level (red circles) and the CdSe $1S_e$ level (blue triangles), respectively. Panel IV: energetic position of both $1S_e$ levels, featuring a separation of 0.52 eV.

Experimental Section for details) is displayed as a gray solid line. A fit consisting of a sum of Gaussians is given as a blue dashed line. Fitted transitions involving the $1S_e$ and $1P_e$ levels are depicted by green and red dashed lines, respectively; higher energy transitions by gray dashed lines. These fits were performed to quantify the bleaches upon electrochemical charging and to correlate them with distinct optical transitions, enabling the assignment of the levels that become occupied.

Differential absorption spectra at potentials ranging from open circuit (−0.3 V) to −1.3 V are given in the bottom panel and color-coded as given in the legend. The $1S_h1S_e$ transition in PbSe at a probe energy of 0.795 eV (red arrow) is bleached from about −0.55 V, whereas the CdSe $1S_{3/2}1S_e$ transition at a probe energy of 1.905 eV (dark blue arrow) bleaches only at potentials exceeding about −0.75 V. The shown differential absorption spectra were collected during the forward scan of the first of two cycles in the CV scan that is shown in Figure 5b-I. In the CV scan a change in slope is observed at −0.55 and −0.80 V on the forward scan coinciding with the appearance of PbSe and CdSe band gap absorption bleaches, respectively, at similar potentials. This suggests that injection into the PbSe and CdSe $1S_e$ states is the dominant current and that the density of localized states is low, or that their charging is so slow that they are not addressed at a scan rate of 10 mV/s of the CV. Negligible charging of localized states is confirmed in the differential capacitance depicted in Figure 5b-II. No charge is injected into the QD film up to −0.50 V, after which two charging waves around −0.65 and −1.00 V are observed, coinciding with the absorption bleaching of the band gap transitions in PbSe and CdSe, respectively.

Figure 5b-III summarizes the optical assessment. An average occupation of one electron per QD is reached at the potentials indicated by horizontal bars in Figure 5b-IV: −4.15 eV vs vacuum for the PbSe $1S_e$ level and −3.63 eV vs vacuum for the CdSe $1S_e$ level. The determined energy level offset of 0.52 eV between CdSe and PbSe in the alternating multilayer film is much higher than the offset of 0.20 eV that we estimated based on the respective levels in the pure films.

In the pure films the QDs are only surrounded by QDs of the same material, while in the multilayer composite films many neighboring QDs will be of the other kind. To check whether this varying environment has a strong influence on the energy level offset, we also constructed bilayer films, consisting of ∼15 monolayers of CdSe QDs on top of ∼15 monolayers of PbSe QDs. In this case both materials are spatially separated and

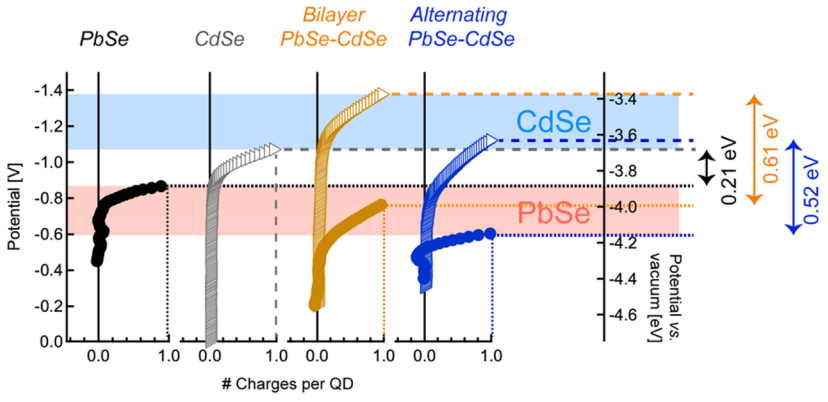

Figure 6. Energy levels and energy level offset depending on layer stack. Number of electrons in the PbSe $1S_e$ level (filled circles) and CdSe $1S_e$ level (open triangles), respectively, for a film of PbSe QDs only (black), CdSe QDs only (gray), a bilayer (yellow), and an alternating multilayer (dark blue). The potential at which the respective $1S_e$ level is occupied by one electron is indicated by dotted (PbSe) and dashed (CdSe) lines, respectively. The spread in potential is illustrated as red and blue shaded area, respectively. The energy level offset based on the single layers (0.21 eV) is much smaller than the energy level offset in the bilayer (0.61 eV) or multilayer (0.52 eV).

DOI: 10.1021/acs.jpcc.5b12016
J. Phys. Chem. C 2016, 120, 5164−5173

their direct environment is similar to the environment in the pure films.

Figure 6 illustrates the number of electrons in the PbSe $1S_e$ level (filled circles) and CdSe $1S_e$ level (open triangles) in pure films of 5.3 nm PbSe QDs (black) and 9.7 nm CdSe QDs (gray) as well as a bilayer (yellow) and an alternating multilayer (blue) of both types of QDs. The experiment with the bilayer is shown in more detail in Figure S2 of the Supporting Information. The Fermi level corresponding to one electron per QD is indicated by dotted and dashed lines for PbSe and CdSe, respectively. It is clear that significant variations exist in the absolute energy levels in the different films. Both the CdSe and PbSe $1S_e$ energy levels vary by about 0.3 eV, in CdSe from −3.68 to −3.38 eV (blue shaded area in Figure 6) and in PbSe from −4.15 eV to −3.88 eV (red shaded area in Figure 6). We observe that the CdSe-PbSe $1S_e$ energy level offset in the multilayer structure (0.52 eV) and the bilayer structure (0.61 eV) are similar, and much larger than what would be inferred from the results obtained on pure films. A control experiment on an inverse bilayer (ITO/CdSe/PbSe), shown in Figure S4 of the Supporting Information, excludes that the difference in energy level offsets arises from different charge injection rates for the various film architectures.

As will be discussed in more detail below, the variation in absolute energy levels is likely due to differences in surface chemistry resulting in a varying extent of surface charging. If for instance more surface charging takes place for PbSe QDs this will cause a larger upward shift of the electron energy levels in PbSe QD films than in CdSe QD films. An energy level offset estimated from the levels of pure PbSe and CdSe QD films will thus contain a contribution of the (different) Coulomb repulsion due to charging. However, in composite CdSe/PbSe QD films surface charges on PbSe QDs also cause an upward shift of the CdSe QD electron energy levels; the latter results in a CdSe $1S_e$ energy level that is higher and an energy level offset that is larger when measured in situ on a composite film, as observed here. Since surface charging causes the energy levels of both PbSe QDs and CdSe QDs to shift in the same direction, energy level offsets are less sensitive to charging effects than the absolute energy levels. These results show that the estimation of energy level offsets in QD heterosystems from energy levels observed for pure films can lead to sizable mistakes and highlight the importance of assessing the energy level offset in situ for the sample of interest.

3.6. Dependence of the Energy Level Offset on the QD Size. Next, we address the dependence of the energy level offset on the size of one of the QDs. To this end, we fabricated bilayers containing a film of CdSe QDs of always the same size on top of a film of PbSe QDs of three distinct sizes: size L with a diameter of 6 nm, size M with a diameter of 5.3 nm, and size S with a diameter of 4.1 nm. The energy level offset of the bilayer with PbSe QDs of size M (0.61 eV) has already been determined in Figure 6. The expectation for the remaining two films is that the offset is larger for PbSe QDs of 6.0 nm diameter and smaller for PbSe QDs of 4.1 nm.

Figure 7a shows the absorption (top panel) and differential absorption spectra (bottom panel) of the film with the larger PbSe QDs of size L. A black solid line shows the absorbance around the $1S_h1S_e$ transition of the PbSe QDs (at 0.69 eV, red arrow) and a gray solid line shows the CdSe contribution around the CdSe $1S_{3/2}1S_e$ transition (at 1.91 eV, dark blue arrow).

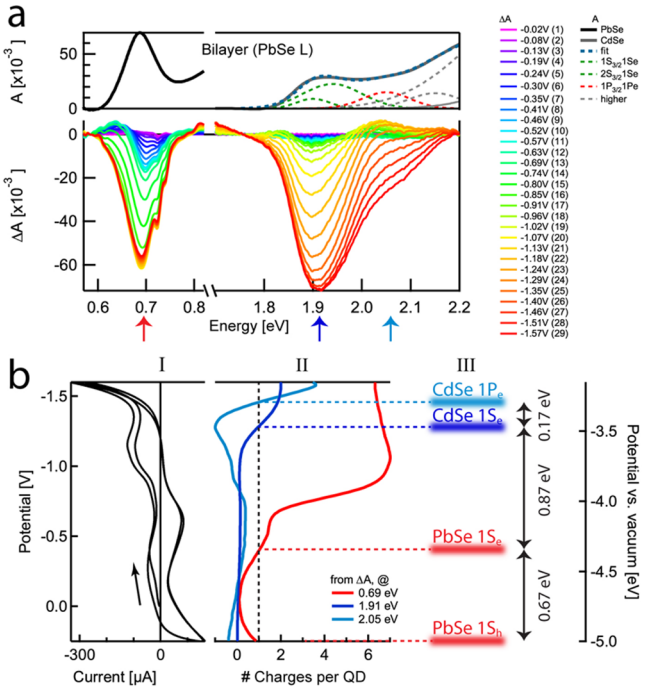

Figure 7. Spectroelectrochemical determination of energy levels in a bilayer of 6.0 nm PbSe QDs (size L, 1S peak at 0.69 eV) and 9.7 nm CdSe QDs (1S peak at 1.91 eV). (a) Upper half: linear absorption spectrum of the bilayer film. In the region from 1.7 to 2.2 eV, only the CdSe contribution to the spectrum is shown and fitted (see main text for details). Lower half: differential absorption spectra for various potentials as indicated in the legend. (b) Panel I: CV, starting from open circuit potential (−0.02 V). An arrow indicates the scan direction. Panel II: number of charges in the PbSe $1S_e$ or $1S_h$ level (red solid line), in the CdSe $1S_e$ level (dark blue solid line), and the CdSe $1P_e$ level (light blue solid line) as deduced from the relative absorption bleach $\Delta A/A$ at 0.69, 1.91, and 2.05 eV, respectively. Panel III: absolute energies of the PbSe $1S_h$ and $1S_e$ level as well as the CdSe $1S_e$ and $1P_e$ level. The level spacing is depicted by arrows.

We now perform a CV scan (see Figure 7b-I), starting from 0 V, beginning in negative scan direction, reversing the potential at −1.6 and +0.25 V, and cycling the potential for two consecutive times. Differential absorption spectra with respect to the absorbance at 0 V are recorded and displayed in Figure 7a. Initially, slight bleaching of the PbSe $1S_h1S_e$ transition is observed, becoming significant from about −0.2 V and almost reaching transparency, i.e., $\Delta A_{1Sh\rightarrow1Se}/A_{1Sh\rightarrow1Se} \approx -1$, at about −1.0 V. The latter indicates that the $1S_e$ levels of the PbSe QDs are almost completely filled (with eight electrons). Bleaching of the $1S_{3/2}1S_e$ and $2S_{3/2}1S_e$ transitions in CdSe occurs at more negative potentials, starting at about −1.0 V and reaching a plateau at about −1.5 V. After the injection of electrons into the $1S_e$ level, also the $1P_e$ level of the CdSe QDs gets charged, as deduced from the increasing absorption bleach at 2.05 V (light blue arrow). Upon reversal of the scan direction, both CdSe and PbSe recover their ground state absorbance, until at positive potentials, the PbSe $1S_h1S_e$ transition gets bleached again, due to hole injection. At a potential of +0.27 V, on average one hole per PbSe QD is injected. Note that due to the limited electrochemical stability at low potentials, hole injection is generally more difficult in QD films. Neither for CdSe QDs nor for smaller PbSe QDs we achieved significant hole injection.

DOI: 10.1021/acs.jpcc.5b12016
J. Phys. Chem. C 2016, 120, 5164−5173

Figure 7b-II depicts the potential dependent number of charges in the $1S_e$ or $1S_h$ level of PbSe (red line), as well as the $1S_e$ level (dark blue line) and $1P_e$ level (light blue line) of CdSe. The energies corresponding to occupation of one charge per QD are shown in Figure 7b-III as horizontal bars versus an absolute energy scale. The PbSe $1S_h$-$1S_e$ interband separation of 0.67 eV (the so-called electrochemical band gap) is in good agreement with the optical band gap of 0.69 eV.

The agreement between the electrochemical and optical band gap demonstrates that the gate coupling, i.e., the ratio of Fermi level shift and applied voltage, is close to unity. This shows that charge compensation by the electrolyte ions is efficient and that the injected charges in the $1S_h$ and $1S_e$ level of PbSe QDs do not influence the energy of these levels (see the Supporting Information). However, a sample-dependent amount of surface charges might eventually lead to a variation in gate coupling (see the discussion below).

For the large PbSe QDs of 6.0 nm, the measured offset between the $1S_e$ levels of CdSe and PbSe amounts to 0.87 eV (see Figure 7b). This is significantly larger than the offset for smaller PbSe QDs of 5.3 nm (0.61 eV, see Figure 6 and Figure S2 in the Supporting Information), consistent with the strong confinement in PbSe nanocrystals, and the concomitant lowering of the $1S_e$ level for larger PbSe QDs.

To verify the trend, we also determined the energy level offset for a bilayer with PbSe QDs of 4.1 nm diameter, amounting to 0.29 eV (see Figure S3 in the Supporting Information). Figure 8a presents an overview of the $1S_e$ electron levels in CdSe and PbSe of all assessed bilayers, depicted by blue triangles and red circles, respectively. All values are plotted with respect to vacuum and as a function of the PbSe band gap. The lowest-energy hole levels of PbSe ($1S_h$) and CdSe ($1S_{3/2}$) were estimated from the respective optical band gaps and are shown as red squares and blue diamonds, respectively. For comparison, also the $1S_e$ and $1S_{3/2}$ energy levels of a pure film of CdSe QDs are appended, as light and dark blue dashed line, respectively.

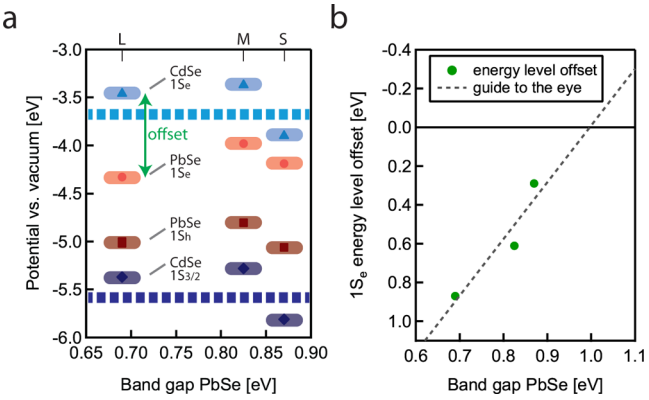

Figure 8. (a) Energy level diagram in PbSe/CdSe QD bilayer films, as a function of the PbSe band gap, for the three studied PbSe sizes L, M, and S. The $1S_e$ levels of CdSe and PbSe are shown as triangles and circles, respectively. The hole levels of CdSe and PbSe are estimated from the respective optical band gaps, shown as diamonds and squares, respectively. The estimated uncertainty of the measurement is depicted by shaded regions. For comparison, the $1S_e$ and $1S_{3/2}$ level of a pure CdSe QD film is depicted as a light and dark blue dashed line, respectively. (b) The $1S_e$ energy level offset between CdSe and PbSe QDs in bilayer films (marked also as double-sided green arrow in subfigure a) is shown as filled green circles. A linear fit of slope −2.9 (gray dashed line) serves as a guide to the eye.

From Figure 8a it is clear that the absolute energy levels are influenced by more than the QD size. The CdSe QDs are all of the same size, but the position of their $1S_e$ level varies by >0.5 eV. Similarly, the $1S_e$ energy level of the PbSe QDs does not decrease with size, as would be expected when going from size S to M to L. However, the expected size-dependent trend is observed for the energy level offset, shown in Figure 8b: the offset increases on going from small to large PbSe QDs. However, a linear fit to the energy level offset with PbSe band gap (dotted line in Figure 8b) has a slope of −2.9. A slope of −0.5 would be expected, if half of the confinement energy in the PbSe band gap is due to the $1S_e$ electron and the other half to the $1S_h$ hole, as is often assumed on the basis of the similar effective masses of electrons and holes in PbSe. Hence, other contributions to the energy level offset must be present.

From all of the above it is clear that the absolute energy levels in these QD films are very sensitive to subtle changes in the films. The fact that the measured energy level offset is similar for multilayer and bilayer PbSe-CdSe QD films suggests that a change in dielectric environment is not the most important factor. In addition, such a change cannot explain the large variations that we observed previously between different pure films,[16] or the large variation of the $1S_e$ level in CdSe QDs for different PbSe QD sizes.

As outlined in the Supporting Information, we estimate that contributions of the electrolyte to the energy of charging, such as attractive Coulomb interactions between injected electrons and ions in the voids of the QDs, are only of the order of −20 meV. Variations in this energy due to differences in the film geometry are expected to be negligible compared to the large variations we observed.

Alternatively, the surface of the QD film may explain differences in the measured energy level structure: the stoichiometry,[34] ligand density,[34,35] ligand anchor group[36−39] as well as charged surface traps[16] have all been shown to shift energy levels. In all our QD films, thiol ligands were used as the organic capping. Thiols are known to affect energy levels of QDs due to surface dipoles.[13,39] However, the same dithiol ligands were used for all films. Therefore, it seems unlikely that subtle changes in the surface density of thiols cause the strong shifts of up to 0.5 eV that we observe.

Rather, we consider that charging of electron traps on the QD surfaces could be the cause of the large energy variations that we observe.[16] Recently we have shown that such traps can be charged when the potential is varied and that this may result in stable, charged QD films.[7,40] Charged surface traps may strongly influence the $1S_e$ energy level by Coulomb repulsion between the trapped electrons and the $1S_e$ electrons. Other indications of surface charging are present in our data: the large hysteresis observed in both the CV measurements and the absorption bleach as well as the onset of charge injection before the observation of a band edge bleach (see, e.g., Figure 3). Similarly, the fact the 1S absorption bleach for PbSe decreases after a certain potential (Figure 3c-III) can be understood by the continuous charging of the surface.

We have argued that cations in the voids of the QD films lead to charge compensation and efficient gate coupling. However, as we have shown previously, there is a maximum number of cations that can be allocated in the QD voids.[20] This number is of the order of 5−10 cations per QD. This means that the addition of more than 5−10 electrons per QDs will be

DOI: 10.1021/acs.jpcc.5b12016
J. Phys. Chem. C 2016, 120, 5164−5173

accompanied by a large increase in Coulomb repulsion. Since typical QDs have hundreds of surface atoms, it is conceivable that there are many surface states per QD. Even a limited number of surface charges per QD can result in an incomplete compensation of this extra charge by the electrolyte ions resulting in an upward shift of the energy levels, as observed in our experiments. Fortunately, such energy shifts will have the same sign for different QDs in QD heterojunctions, such that they cancel, at least in part, in the in situ measurement of energy level offsets.

4. CONCLUSIONS

We have demonstrated that spectroelectrochemistry can be used for the in situ determination of energy level offsets in QD films. We fabricated PbSe and CdSe QD heterojunctions, both as a bilayer and as an alternating multilayer film, showing a similar (type I) energy level offset, with the $1S_e$ level 0.2−0.9 eV higher in CdSe than in PbSe QDs, depending on the size of the QDs. Significant variations in the absolute energy levels are observed between different samples, most likely as a result of varying defect densities resulting in a varying extent of surface charging. This makes extrapolation of energy level offsets from reference films of the pure QDs inaccurate. It was shown, however, that energy level offsets in in situ measurements are less sensitive to such variations. The spectroelectrochemical technique to determine band offsets in heterojunctions is in principle applicable to other material systems as well. A prerequisite is that the materials are porous enough to allow the uptake of counterions that compensate the introduced charges efficiently.[16,20] Examples are films of conducting polymers,[41] films of carbon nanotubes,[42] or even solids that allow for intercalation of ions.[43]

■ ASSOCIATED CONTENT

Supporting Information

The Supporting Information is available free of charge on the ACS Publications website at DOI: 10.1021/acs.jpcc.5b12016.

Energetics of electron injection. Optical versus electrochemical band gap. Spectroelectrochemical assessment of energy levels in bilayers of PbSe and CdSe QDs. Processing of absorption data in spectroelectrochemical measurements. Spectroelectrochemical assessment of energy levels in an inverse bilayer of PbSe and CdSe QDs. Reproducibility of spectroelectrochemical measurements. Effect of water and air on spectroelectrochemical measurements. (PDF)

■ AUTHOR INFORMATION

Corresponding Authors

*E-mail: S.C.Boehme@vu.nl.

*E-mail: A.J.Houtepen@tudelft.nl.

Present Address

[‖]LaserLaB Amsterdam, Vrije Universiteit Amsterdam, De Boelelaan 1081, 1081 HV Amsterdam, The Netherlands.

Author Contributions

S.C.B. performed and A.J.H. devised the experiments. W.H.E. and S.C.B. prepared the samples. S.C.B and A.J.H. wrote the paper. W.H.E., D.V., and L.D.A.S. aided in the interpretations of the results. All authors have given approval to the final version of the manuscript.

Notes

The authors declare no competing financial interest.

■ ACKNOWLEDGMENTS

We thank M.J.W. Vermeulen, J.W.A. Suijkerbuijk, and N. Alberts for help with realizing the experimental setup and C.S. Suchand Sandeep for help with the sample preparation. This work is part of the Joint Solar Programme (JSP) of HyET Solar and the Stichting voor Fundamenteel Onderzoek der Materie (FOM), which is part of The Netherlands Organisation for Scientific Research (NWO).

■ REFERENCES

(1) Katoh, R.; Furube, A.; Barzykin, A. V.; Arakawa, H.; Tachiya, M. Kinetics and Mechanism of Electron Injection and Charge Recombination in Dye-Sensitized Nanocrystalline Semiconductors. *Coord. Chem. Rev.* **2004**, *248*, 1195−1213.

(2) Tisdale, W. A.; Zhu, X.-Y. Artificial Atoms on Semiconductor Surfaces. *Proc. Natl. Acad. Sci. U. S. A.* **2011**, *108*, 965−970.

(3) Tvrdy, K.; Frantsuzov, P. A.; Kamat, P. V. Photoinduced Electron Transfer from Semiconductor Quantum Dots to Metal Oxide Nanoparticles. *Proc. Natl. Acad. Sci. U. S. A.* **2011**, *108*, 29−34.

(4) Zhu, H.; Song, N.; Lian, T. Controlling Charge Separation and Recombination Rates in Cdse/Zns Type I Core−Shell Quantum Dots by Shell Thicknesses. *J. Am. Chem. Soc.* **2010**, *132*, 15038−15045.

(5) Wang, H.; McNellis, E. R.; Kinge, S.; Bonn, M.; Cánovas, E. Tuning Electron Transfer Rates through Molecular Bridges in Quantum Dot Sensitized Oxides. *Nano Lett.* **2013**, *13*, 5311−5315.

(6) Knowles, K. E.; Malicki, M.; Weiss, E. A. Dual-Time Scale Photoinduced Electron Transfer from Pbs Quantum Dots to a Molecular Acceptor. *J. Am. Chem. Soc.* **2012**, *134*, 12470−12473.

(7) Boehme, S. C.; Walvis, T. A.; Infante, I.; Grozema, F. C.; Vanmaekelbergh, D.; Siebbeles, L. D. A.; Houtepen, A. J. Electrochemical Control over Photoinduced Electron Transfer and Trapping in Cdse-Cdte Quantum-Dot Solids. *ACS Nano* **2014**, *8*, 7067−7077.

(8) Marcus, R. A. On the Theory of Oxidation-Reduction Reactions Involving Electron Transfer. I. *J. Chem. Phys.* **1956**, *24*, 966−978.

(9) Marcus, R. A. Electrostatic Free Energy and Other Properties of States Having Nonequilibrium Polarization. I. *J. Chem. Phys.* **1956**, *24*, 979−989.

(10) Marcus, R. A. On the Theory of Electron-Transfer Reactions. Vi. Unified Treatment for Homogeneous and Electrode Reactions. *J. Chem. Phys.* **1965**, *43*, 679−701.

(11) Marcus, R. A.; Sutin, N. Electron Transfers in Chemistry and Biology. *Biochim. Biophys. Acta, Rev. Bioenerg.* **1985**, *811*, 265−322.

(12) Pandey, A.; Guyot-Sionnest, P. Intraband Spectroscopy and Band Offsets of Colloidal Ii-Vi Core/Shell Structures. *J. Chem. Phys.* **2007**, *127*, 104710.

(13) Munro, A. M.; Zacher, B.; Graham, A.; Armstrong, N. R. Photoemission Spectroscopy of Tethered Cdse Nanocrystals: Shifts in Ionization Potential and Local Vacuum Level as a Function of Nanocrystal Capping Ligand. *ACS Appl. Mater. Interfaces* **2010**, *2*, 863−869.

(14) Jasieniak, J.; Califano, M.; Watkins, S. E. Size-Dependent Valence and Conduction Band-Edge Energies of Semiconductor Nanocrystals. *ACS Nano* **2011**, *5*, 5888−5902.

(15) Gao, J.; Luther, J. M.; Semonin, O. E.; Ellingson, R. J.; Nozik, A. J.; Beard, M. C. Quantum Dot Size Dependent J-V Characteristics in Heterojunction Zno/Pbs Quantum Dot Solar Cells. *Nano Lett.* **2011**, *11*, 1002−1008.

(16) Houtepen, A. J.; Vanmaekelbergh, D. Orbital Occupation in Electron-Charged Cdse Quantum-Dot Solids. *J. Phys. Chem. B* **2005**, *109*, 19634−19642.

(17) Vanmaekelbergh, D.; Houtepen, A. J.; Kelly, J. J. Electrochemical Gating: A Method to Tune and Monitor the (Opto)-Electronic Properties of Functional Materials. *Electrochim. Acta* **2007**, *53*, 1140−1149.

DOI: 10.1021/acs.jpcc.5b12016
J. Phys. Chem. C 2016, 120, 5164−5173

(18) Guyot-Sionnest, P. Charging Colloidal Quantum Dots by Electrochemistry. *Microchim. Acta* **2008**, *160*, 309−314.
(19) Guyot-Sionnest, P.; Wang, C. Fast Voltammetric and Electrochromic Response of Semiconductor Nanocrystal Thin Films. *J. Phys. Chem. B* **2003**, *107*, 7355−7359.
(20) Boehme, S. C.; Wang, H.; Siebbeles, L. D. A.; Vanmaekelbergh, D.; Houtepen, A. J. Electrochemical Charging of Cdse Quantum Dot Films: Dependence on Void Size and Counterion Proximity. *ACS Nano* **2013**, *7*, 2500−2508.
(21) Jones, M.; Kumar, S.; Lo, S. S.; Scholes, G. D. Exciton Trapping and Recombination in Type Ii Cdse/Cdte Nanorod Heterostructures. *J. Phys. Chem. C* **2008**, *112*, 5423−5431.
(22) Wehrenberg, B. L.; Guyot-Sionnest, P. Electron and Hole Injection in Pbse Quantum Dot Films. *J. Am. Chem. Soc.* **2003**, *125*, 7806.
(23) Mekis, I.; Talapin, D. V.; Kornowski, A.; Haase, M.; Weller, H. One-Pot Synthesis of Highly Luminescent Cdse/Cds Core-Shell Nanocrystals Via Organometallic and "Greener" Chemical Approaches. *J. Phys. Chem. B* **2003**, *107*, 7454−7462.
(24) de Mello Donegá, C.; Koole, R. Size Dependence of the Spontaneous Emission Rate and Absorption Cross Section of Cdse and Cdte Quantum Dots. *J. Phys. Chem. C* **2009**, *113*, 6511−6520.
(25) Steckel, J. S.; Yen, B. K. H.; Oertel, D. C.; Bawendi, M. G. On the Mechanism of Lead Chalcogenide Nanocrystal Formation. *J. Am. Chem. Soc.* **2006**, *128*, 13032−13033.
(26) Ruch, P. W.; Cericola, D.; Hahn, M.; Kötz, R.; Wokaun, A. On the Use of Activated Carbon as a Quasi-Reference Electrode in Non-Aqueous Electrolyte Solutions. *J. Electroanal. Chem.* **2009**, *636*, 128−131.
(27) Wang, Y.; Rogers, E. I.; Compton, R. G. The Measurement of the Diffusion Coefficients of Ferrocene and Ferrocenium and Their Temperature Dependence in Acetonitrile Using Double Potential Step Microdisk Electrode Chronoamperometry. *J. Electroanal. Chem.* **2010**, *648*, 15−19.
(28) Neamen, D. A. *Semiconductor Physics and Devices: Basic Principles*; McGraw-Hill: New York, 2003.
(29) Roest, A. L.; Kelly, J. J.; Vanmaekelbergh, D. Coulomb Blockade of Electron Transport in a Zno Quantum-Dot Solid. *Appl. Phys. Lett.* **2003**, *83*, 5530−5532.
(30) Wehrenberg, B. L.; Yu, D.; Ma, J.; Guyot-Sionnest, P. Conduction in Charged Pbse Nanocrystal Films. *J. Phys. Chem. B* **2005**, *109*, 20192−20199.
(31) Schins, J. M.; Trinh, M. T.; Houtepen, A. J.; Siebbeles, L. D. A. Probing Formally Forbidden Optical Transitions in Pbse Nanocrystals by Time- and Energy-Resolved Transient Absorption Spectroscopy. *Phys. Rev. B: Condens. Matter Mater. Phys.* **2009**, *80*, 035323.
(32) Trinh, M. T.; Houtepen, A. J.; Schins, J. M.; Piris, J.; Siebbeles, L. D. A. Nature of the Second Optical Transition in Pbse Nanocrystals. *Nano Lett.* **2008**, *8*, 2112−2117.
(33) Norris, D. J.; Bawendi, M. G. Measurement and Assignment of the Size-Dependent Optical Spectrum in Cdse Quantum Dots. *Phys. Rev. B: Condens. Matter Mater. Phys.* **1996**, *53*, 16338−16346.
(34) Anderson, N. C.; Hendricks, M. P.; Choi, J. J.; Owen, J. S. Ligand Exchange and the Stoichiometry of Metal Chalcogenide Nanocrystals: Spectroscopic Observation of Facile Metal-Carboxylate Displacement and Binding. *J. Am. Chem. Soc.* **2013**, *135*, 18536−18548.
(35) Kim, D.; Kim, D.-H.; Lee, J.-H.; Grossman, J. C. Impact of Stoichiometry on the Electronic Structure of Pbs Quantum Dots. *Phys. Rev. Lett.* **2013**, *110*, 196802.
(36) Nag, A.; Chung, D. S.; Dolzhnikov, D. S.; Dimitrijevic, N. M.; Chattopadhyay, S.; Shibata, T.; Talapin, D. V. Effect of Metal Ions on Photoluminescence, Charge Transport, Magnetic and Catalytic Properties of All-Inorganic Colloidal Nanocrystals and Nanocrystal Solids. *J. Am. Chem. Soc.* **2012**, *134*, 13604−13615.
(37) Chuang, C.-H. M.; Brown, P. R.; Bulović, V.; Bawendi, M. G. Improved Performance and Stability in Quantum dot Solar Cells through Band Alignment engineering. *Nat. Mater.* **2014**, *13*, 796−801.
(38) Ning, Z.; et al. Air-Stable N-Type Colloidal Quantum Dot Solids. *Nat. Mater.* **2014**, *13*, 822−828.
(39) Yaacobi-Gross, N.; Soreni-Harari, M.; Zimin, M.; Kababya, S.; Schmidt, A.; Tessler, N. Molecular Control of Quantum-Dot Internal Electric Field and Its Application to Cdse-Based Solar Cells. *Nat. Mater.* **2011**, *10*, 974−979.
(40) Boehme, S. C.; Azpiroz, J. M.; Aulin, Y. V.; Grozema, F. C.; Vanmaekelbergh, D.; Siebbeles, L. D. A.; Infante, I.; Houtepen, A. J. Density of Trap States and Auger-Mediated Electron Trapping in Cdte Quantum-Dot Solids. *Nano Lett.* **2015**, *15*, 3056−3066.
(41) Hulea, I. N.; Brom, H. B.; Houtepen, A. J.; Vanmaekelbergh, D.; Kelly, J. J.; Meulenkamp, E. A. Wide Energy-Window View on the Density of States and Hole Mobility in Poly(P-Phenylene Vinylene). *Phys. Rev. Lett.* **2004**, *93*, 166601.
(42) Ozel, T.; Gaur, A.; Rogers, J. A.; Shim, M. Polymer Electrolyte Gating of Carbon Nanotube Network Transistors. *Nano Lett.* **2005**, *5*, 905−911.
(43) Natan, M. J.; Mallouk, T. E.; Wrighton, M. S. The Ph-Sensitive Tungsten(Vi) Oxide-Based Microelectrochemical Transistors. *J. Phys. Chem.* **1987**, *91*, 648−654.

DOI: 10.1021/acs.jpcc.5b12016
J. Phys. Chem. C 2016, 120, 5164−5173